False Alarm Control of CFAR Algorithms with Experimental Bistatic Radar Data

Tri-Tan V. Cao, James Palmer, Paul E. Berry
Defence Science & Technology Organization (DSTO)
180L, DSTO Edinburgh, PO Box 1500, SA 5111
Adelaide, Australia

***Abstract*—False alarm control performance of different constant false alarm rate (CFAR) algorithms is experimentally investigated using bistatic radar data. The CFARs under investigation include cell-averaging (CA-CFAR), smaller-of (SO-CFAR), greater-of (GO-CFAR), ordered-statistic (OS-CFAR), censored cell-averaging (CCA-CFAR), and the homogeneity detector mean-to-mean ratio (MMR) test. The experimental data was collected using an Illuminator of Opportunity (IOO) bistatic radar that is under ongoing development at DSTO. For this set of experimental data, it is observed that CFAR algorithms that have a higher CFAR loss in a homogeneous environment will have a larger theory-experiment false alarm mismatch, especially at smaller false alarm rates and larger CFAR window sizes.**

I. INTRODUCTION

A radar detection process involves testing whether the signal level in the resolution cell under test exceeds a detection threshold. To be useful in practice, a radar detector not only should be able to detect targets with high probability but also should simultaneously control the false alarm rate at a specified value. In modern radar systems, the false alarm rate is automatically maintained at a constant level by adaptively adjusting the detection threshold according to the background clutter and noise using a constant false alarm rate (CFAR) detector [1].

A wealth of CFAR detection algorithms have been proposed in the literature, for reference see [2]. In general, the signal level in the test cell (in which a decision on target presence or absence is to be made) is compared with an interference level estimate that is determined from the signal levels in a set of cells known as reference cells (which are in the vicinity of the test cell). Different CFAR algorithms have different methods of interference estimation. The majority of CFAR algorithms, however, rely on the assumption that the samples in the reference cells are statistically independent and identically distributed (i.i.d.).

It should be noted that the i.i.d. assumption is not always valid in practice. The reason for this is two-fold: firstly, there are real radar scenarios in which there can be an abrupt change in the statistical property of the reference samples, for example, at the border between land and sea; and secondly, there is no guarantee that the probability density function (pdf) that characterizes the experimental data matches exactly with the theoretically assumed pdf.

Therefore, it is important to assess how well different CFAR detectors comply with the theoretical false alarm control specification when they are applied to experimental data. This is the aim of this paper for a small subset of bistatic radar data.

The CFAR algorithms under investigation are [2]: cell-averaging CFAR (CA-CFAR), smaller-of CFAR (SO-CFAR), greater-of CFAR (GO-CFAR), ordered-statistic CFAR (OS-CFAR), censored cell-averaging CFAR (CCA-CFAR) and the recently proposed homogeneity detector mean-to-mean ratio (MMR) test [3-4]. This study is based on the assumption that all samples in the test cell and the reference cells are Rayleigh distributed. CA-CFAR is known to be optimal with i.i.d. Rayleigh interference, in the sense that the detector gives the highest detection probability for a given false alarm rate. SO-CFAR is well-known for its detection performance against targets near a clutter edge, while GO-CFAR is capable of controlling the false alarm inflation right at that clutter edge. OS-CFAR is a unique CFAR detector that gives a detection threshold that is a linear scale of a sample in a single reference cell. These CFAR algorithms are ranked from low to high in terms of CFAR loss as follows [5]: CA, GO, CCA, OS, SO. Here CFAR loss is defined as the additional signal-to-noise ratio (SNR) a CFAR detector requires in order to achieve the same detection probability as compared to the other CFAR algorithms. Note that although the MMR test has the CFAR property, it is not designed to detect targets in the test cell, but to determine whether the samples in the CFAR window are statistically identical.

The aforementioned CFAR algorithms have been applied to the experimental data collected from an Illuminator of Opportunity (IOO) bistatic radar that is under ongoing development at DSTO. The application of bistatic radar has a number of advantages over monostatic radar, especially when

978-1-4244-5813-4/10/$26.00 ©2010 IEEE

Report Documentation Page

Form Approved
OMB No. 0704-0188

1. REPORT DATE	2. REPORT TYPE	3. DATES COVERED
MAY 2010		**00-00-2010 to 00-00-2010**

4. TITLE AND SUBTITLE	5a. CONTRACT NUMBER
False Alarm Control of CFAR Algorithms with Experimental Bistatic Radar Data	5b. GRANT NUMBER
	5c. PROGRAM ELEMENT NUMBER
6. AUTHOR(S)	5d. PROJECT NUMBER
	5e. TASK NUMBER
	5f. WORK UNIT NUMBER
7. PERFORMING ORGANIZATION NAME(S) AND ADDRESS(ES) **Defence Science & Technology Organization (DSTO),180L, DSTO Edinburgh,PO Box 1500,SA 5111 Adelaide, Australia,**	8. PERFORMING ORGANIZATION REPORT NUMBER
9. SPONSORING/MONITORING AGENCY NAME(S) AND ADDRESS(ES)	10. SPONSOR/MONITOR'S ACRONYM(S)
	11. SPONSOR/MONITOR'S REPORT NUMBER(S)

12. DISTRIBUTION/AVAILABILITY STATEMENT
Approved for public release; distribution unlimited

13. SUPPLEMENTARY NOTES
See also ADM002322. Presented at the 2010 IEEE International Radar Conference (9th) Held in Arlington, Virginia on 10-14 May 2010. Sponsored in part by the Navy.

14. ABSTRACT
False alarm control performance of different constant false alarm rate (CFAR) algorithms is experimentally investigated using bistatic radar data. The CFARs under investigation include cell-averaging (CA-CFAR), smaller-of (SOCFAR) greater-of (GO-CFAR), ordered-statistic (OS-CFAR) censored cell-averaging (CCA-CFAR), and the homogeneity detector mean-to-mean ratio (MMR) test. The experimental data was collected using an Illuminator of Opportunity (IOO) bistatic radar that is under ongoing development at DSTO. For this set of experimental data, it is observed that CFAR algorithms that have a higher CFAR loss in a homogeneous environment will have a larger theory-experiment false alarm mismatch, especially at smaller false alarm rates and larger CFAR window sizes.

15. SUBJECT TERMS

16. SECURITY CLASSIFICATION OF:			17. LIMITATION OF ABSTRACT	18. NUMBER OF PAGES	19a. NAME OF RESPONSIBLE PERSON
a. REPORT **unclassified**	b. ABSTRACT **unclassified**	c. THIS PAGE **unclassified**	**Same as Report (SAR)**	**6**	

IOO are employed for passive coherent location. For example, an IOO bistatic radar does not require a dedicated transmitter, which significantly reduces its implementation costs. Also, a targets' bistatic radar cross section is different [6] to its monostatic RCS, which may assist in target detection and/or classification.

The paper is organized as follows. A summary of the CFAR algorithms under consideration is given in Section II, followed by brief description of the IOO bistatic radar data in Section III. The theoretical and experimental results as well as the discussions are then given in Sections IV. Conclusions and a discussion of future work are provided in Section V.

II. Description of CFAR Algorithms

A. Signal and Interference Model

Consider a radar range-Doppler map as described by matrix A in Figure 1. Data in the same row of A represent samples in the same Doppler filter, whereas data in the same column of A are assumed time-coincident (i.e., representing samples at the same range gate). Assume that samples in the range-Doppler map are output of a squared-law detector and are statistically independent. Assume also that the amplitude of each sample can be described by the following exponential probability density function (pdf):

$$p_z(z) = (1/\lambda)\exp(-z/\lambda), \quad z \geq 0 \tag{1}$$

where:
(i) $\lambda=\lambda_N$ if the sample is thermal noise only where $\lambda_N/2$ is the thermal noise power;
(ii) $\lambda=\lambda_N(1+\sigma)$ if the sample contains a target return with an average SNR of σ;
(iii) $\lambda=\lambda_N(1+C)$ if the sample contains a clutter return with an average interference-to-noise ratio (INR) of C;
It should be noted that Swerling I targets in a Rayleigh background are assumed [2]. In this paper, cases (ii) and (iii) shall be considered target-like.

B. Detection Procedure

Target CFAR detection is performed at each resolution cell in the range-Doppler map using a sliding window along each row of the matrix A as shown in Figure 1.

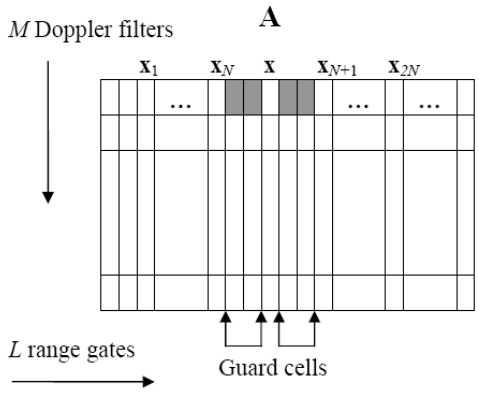

Figure 1: Data in a range-Doppler map

To test if a target is present at range gate x, also known as the test cell, a few immediate neighbouring range gates are used as a guard to avoid signal spillover from x. Data from $2N$ range gates outside the guard region: $x_1, x_2,\ldots, x_N$ on the left and $x_{N+1}, x_{N+2}, \ldots, x_{2N}$ on the right (ie., N range gates on each side of x), are used to compute the detection threshold. The following two alternative hypothesises are to be verified:

H_0: the sample in the test cell is thermal noise only (case i), or

H_1: the sample in the test cell contains a target-like signal (cases ii & iii).

This hypothesis verification is performed as follows:

$$x \underset{H_0}{\overset{H_1}{\gtrless}} \textit{Detection Threshold} \tag{2}$$

i.e., hypothesis H_1 is verified (target present) if the sample x in the test cell exceeds the detection threshold; otherwise ($x \leq$ Detection Threshold) hypothesis H_0 is verified (target absent).

C. Description of CFAR Detectors

CA-CFAR: $\textit{Detection Threshold} = T \times \sum_{n=1}^{2N} x_n$

SO-CFAR: $\textit{Detection Threshold} = T \times \min\left(\sum_{n=1}^{N} x_n, \sum_{n=N+1}^{2N} x_n\right)$

GO-CFAR: $\textit{Detection Threshold} = T \times \max\left(\sum_{n=1}^{N} x_n, \sum_{n=N+1}^{2N} x_n\right)$

OS-CFAR: $\textit{Detection Threshold} = T \times x_{(k)}$

CCA-CFAR: $\textit{Detection Threshold} = T \times \sum_{n=1}^{k} x_{(n)}$ (3)

where T is a constant multiplier that is dependent on the required false alarm rate; $x_{(1)} \leq x_{(2)} \leq \ldots \leq x_{(k)} \leq \ldots \leq x_{(2N)}$ are the ordered reference samples; and for OS- and CCA-CFAR, k defines the k^{th} ranked sample employed in the interference estimation.

The MMR test is performed as follows. For a given set of $2N$ reference samples $\Omega = \{x_1, x_2, \ldots, x_{2N}\}$, let $\Omega_1 = \{ x_n \in \Omega \mid x_n > \text{mean}(\Omega) \}$, $\Omega_0 = \{ x_n \in \Omega \mid x_n \leq \text{mean}(\Omega) \}$, $\mu_1 = \text{mean}(\Omega_1)$, and $\mu_0 = \text{mean}(\Omega_0)$, the MMR test is then:

$$\frac{\mu_1}{\mu_0} \underset{H_{00}}{\overset{H_{11}}{\gtrless}} T \tag{4}$$

where: H_{00}: all samples in Ω are noise only, or

H_{11}: at least one sample in Ω is target-like.

III. The Experimental Bistatic Radar Data

To experimentally investigate the false alarm control performance of the CFAR detectors under consideration, seven bistatic radar data files were employed. Each dataset is known to contain several targets of opportunity. The size of each data file is summarized in Table I. For instance, data file

Bistat_174b consists of 299 consecutive frames (range-Doppler maps, equivalent to a Coherent Processing Interval (CPI)), each of which is a matrix of 835 range columns and 128 Doppler rows as described by matrix A of Figure 1. The datasets were collected using a custom receiver that was designed (primarily using Commercial Off the Shelf (COTS) components) and built by the Defence Science and Technology Organisation (DSTO) of Australia. The receiver, which belongs to the eXperimental Phased Array Radar (XPAR) project, digitises and extracts RF signals to a recording device for offline digital signal processing. The XPAR receiver RF chain down-converts the received signal from up to 16 independent elements to a 175MHz nominal Intermediate Frequency (IF). Each array element has a separate 14-bit Analogue-to-Digital converter (ADC) that allows the IF signal to be digitised at 100MS/s. The XPAR system then uses COTS chipsets to digitally down-convert the IF signal to baseband where the samples are stored on a large non-volatile disk in 32-bit complex values. The XPAR receiver's RF chain is displayed in Figure 2.

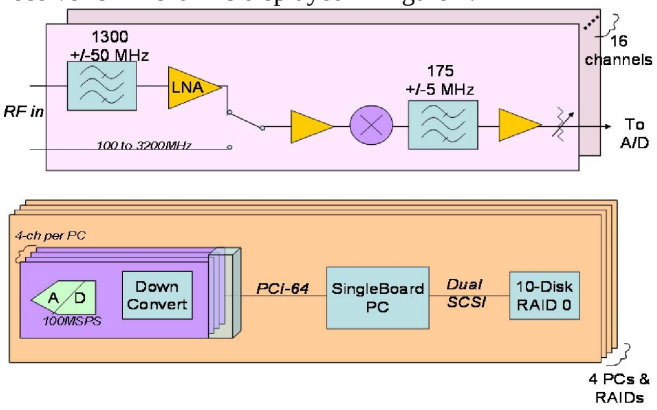

Figure 2: The XPAR receiver RF chain

The XPAR receiver was deployed near an airfield and with an unimpeded Line of Sight (LOS) look direction to Mt Lofty (location of Adelaide's primary Terrestrial Digital Video Broadcast (DVB-T) transmitters). The receiver was deployed in a two-channel configuration: one channel dedicated to LOS signal reception, and the other used for target surveillance. Each channel used a directive Yagi-Uda antenna, and the surveillance antenna received the LOS signal through an antenna backlobe. This configuration permitted integration via 2D cross-correlation (c.f. Eqn 5) with a minimum of target energy in the LOS channel, and vice versa.

$$|\chi(\tau,\nu)|^2 = \left| \int_T r_{LOS}(t) \cdot r_T^*(t-\tau) \exp(-j2\pi\nu t)\, dt \right|^2 \quad (5)$$

where χ is the cross ambiguity value, τ is the delay, ν is the Doppler, r_{LOS} is the LOS reference signal and r_T is the surveillance channel signal. The targets were primarily detected in a "Transmitter over the shoulder of the Receiver" configuration as shown in Figure 3; principally because this was the sector that provided a target rich environment. An example range-Doppler map showing an airborne target is presented in Figure 4.

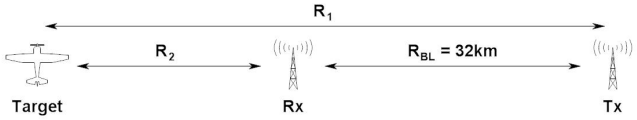

Figure 3: Deployed radar configuration

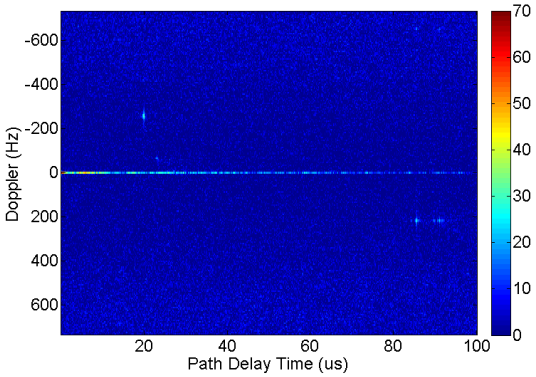

Figure 4: Range-Doppler map showing targets, clutter and ambiguities

The corresponding CA-CFAR detection map (of a single CPI – false alarm rate of 10^{-6}) is shown in Figure 5, and the collapsed time CFAR detection history of the full dataset is shown in Figure 6. It should be noted that the static clutter has been rejected in these figures due to its relatively uniform distribution along the zero Doppler line.

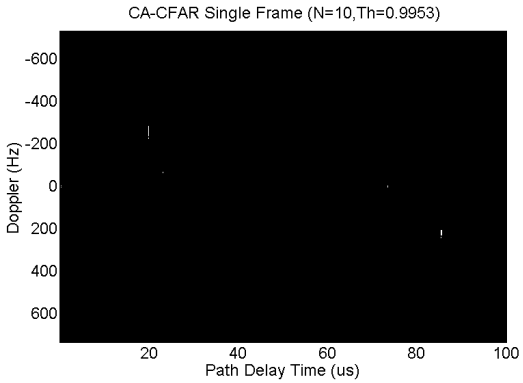

Figure 5: Single CPI CA-CFAR detection of airborne target

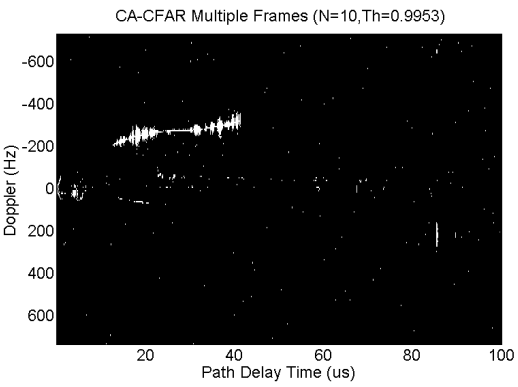

Figure 6: CA-CFAR of multiple CPIs

Figure 4, Figure 5 and Figure 6 illustrate the target detection performance of the CA-CFAR algorithm on a single dataset. Whilst a large amount of static clutter and a number of ambiguities (principally starting at approximately 85μs and 200Hz) appear in Figure 4, the corresponding detection plot shows practically no clutter and a significant reduction in the presence of ambiguities (although one does still exist). As is evident from Figure 6 though, the remaining ambiguity does not behave in a target-like manner as it appears static throughout time even though it has a Doppler offset. In Figure 6 a number of slow moving targets are also apparent as well as the dominant "track" of the airborne target. Whilst these figures visually demonstrate the performance of one of the CFAR algorithms being considered in this paper on a single dataset, they do not provide a clear analytical measure or an indication of performance across multiple CFAR thresholds or datasets. These results will be presented in the following section.

IV. Results & Discussions

To plot the experimental false alarm curves, the most homogeneous regions without targets in those data files are selected. For each file, approximately between 1.3×10^7 to 1.4×10^7 detection trials are performed using a CFAR detection window which slides along each range profile (i.e. along each row of the range-Doppler map A shown in Figure 1).

TABLE I. Description of Bistatic Data Files

File name	Size		
	Frame	***Range***	***Doppler***
Bistat_174a	300	835	128
Bistat_174b	299	835	128
Bistat_176a	300	1043	128
Bistat_176b	299	1043	128
Bistat_180a	300	1043	128
Bistat_180b	299	1043	128
Bistat_181	99	1668	128

For theory-experiment comparison, the theoretically predicted false alarm curves are also plotted. Except the case of CCA-CFAR and MMR-CFAR the false alarm curves of which are obtained using Monte-Carlo method with random number generator and 10^7 trials at each data point, the theoretical false alarm curves of other CFARs are plotted using the closed-form formulas derived in [2].

The experimental false alarm rates for different CFAR detectors are shown in Figure 7 - Figure 12. For OS- and CCA-CFAR, $k=1.5N$ was selected.

Overall, it is found that CA-CFAR has an experimental false alarm control performance that agrees very well with what predicted in theory. For the seven experimental data files, file Bistat_181 gives the best theory-experiment match, while file Bistat_174b gives the worst theory-experiment deviation as shown in Figure 7.

GO-CFAR also gives a very good theory-experiment match as shown in Figure 8 in which a similar false alarm match like that of the CA-CFAR is evident. The match is found over the whole false alarm range from 10^{-1} to 10^{-6} and over a wide spectrum of CFAR window size from $2N=8$ to 40.

For CCA-CFAR of Figure 9, the experimental false alarm curves follow the theoretical ones closely, but there is a noticeable deviation at lower false alarm values (for instance, below 10^{-4}) and at higher CFAR window sizes (for instance, when $2N \geq 24$).

OS-CFAR performs similarly to CCA-CFAR, although there is a more remarkable theory-experiment discrepancy at CFAR window size $2N=8$ as shown in Figure 10.

SO-CFAR has the worst theory-experiment false alarm mismatch as shown in Figure 11. The discrepancy remarkably increases when the CFAR window size $2N\geq24$.

For MMR-CFAR of Figure 12, it is evident that the experimental false alarm curves do not match well with the theoretical ones. For instance, at false alarm rate of 10^{-5}, the experiment-to-theory false alarm ratios are 2, 5, and 10 for CFAR windows $2N=12$, 24, and 40, respectively.

For this experimental bistatic data set, CA-CFAR gives the best theory-experiment false alarm agreement. It is observed that a CFAR algorithm that has a higher CFAR detection loss in a homogeneous environment will have larger theory-experiment false alarm mismatches, especially at smaller false alarm rates and larger CFAR window sizes.

The distribution of data file Bistat_174b is plotted on Weibull paper [7] as shown in Figure 13. The slope of the straight line is 1, which is a clear confirmation of Rayleigh distribution. The correlation of the same data is shown in Figure 14, from which a correlation of up to 6 range-delay samples is evident. Although not shown here, Rayleigh statistic is also observed in other 6 data files with the same correlation of up to 6 range-delay samples.

The false alarm probability of SO-CFAR is now computed for file Bistat_174b using range-delay samples that are $p=1$, 2, and 5 samples apart. The results are shown in Figure 15. As p increases from 1 to 5, the theory-experiment mismatch becomes smaller. When $p=5$, an almost perfect match is obtained. The reason is that the range-delay samples are less correlated when they are further apart while the same Rayleigh distribution is still valid. Also shown in Figure 15 are the false alarm curves of GO-CFAR which are approximately the same for $p=1$, 2, and 5. Although not shown in this paper, the same behaviour is also observed for the MMR-CFAR test.

One explanation for the correlation of the data is a result of the waveform ambiguity function of the DVB-T signal. The DVB-T signal is best described as having a thumbtack waveform ambiguity function; good resolution in range and Doppler but poor dynamic range performance due to the presence of a pedestal that extends in all range and Doppler around the central spike. Given the high level of DPI and static clutter present in these datasets (as evidenced by Figure 4), it means that targets are not actually being detected against thermal noise, but against the pedestal of the strongest signal. Interestingly enough, as these results show, the pedestal of the waveform ambiguity function behaves remarkably like

thermal noise for the majority of thresholds and CFAR algorithms considered.

V. Conclusions and Future Work

In this paper, the false alarm control performance of six CFAR detectors is experimentally investigated using bistatic radar data; the statistics of which are correlated Gaussian. CA-CFAR is found to have the best theory-experiment false alarm agreement. It is observed that for this set of experimental data, in general CFAR algorithms that have higher CFAR detection losses in a homogeneous environment will have larger theory-experiment false alarm mismatches, especially at smaller false alarm rates and larger CFAR window sizes.

Future research into the application of these CFAR algorithms to IOO bistatic radar data will include signal processing means of reducing the Direct Path Interference and static clutter's pedestal signal levels down to the thermal noise or below in order to determine what impact this has on the algorithm's performance.

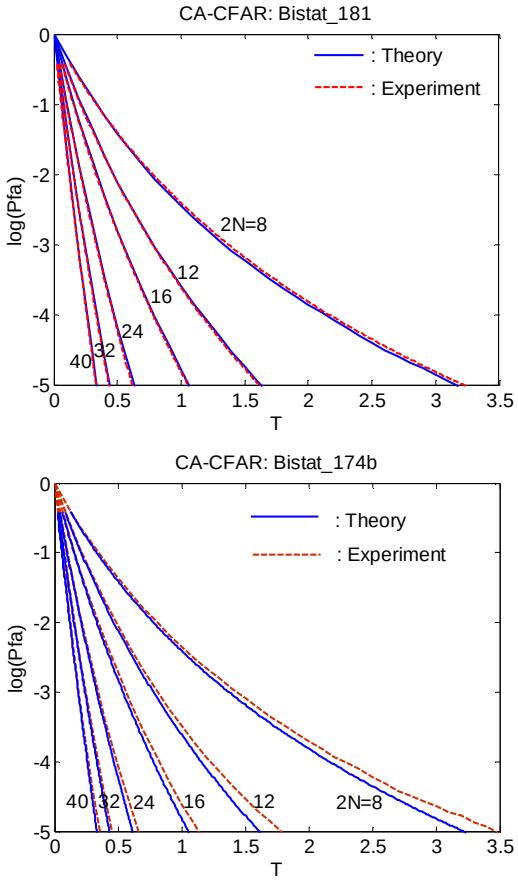

Figure 7: False alarm control of CA-CFAR

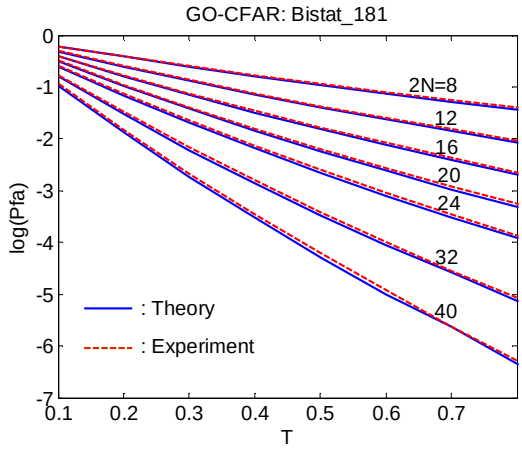

Figure 8: False alarm control of GO-CFAR

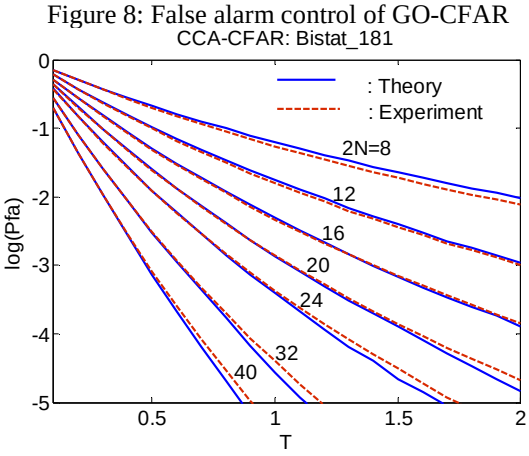

Figure 9: False alarm control of CCA-CFAR

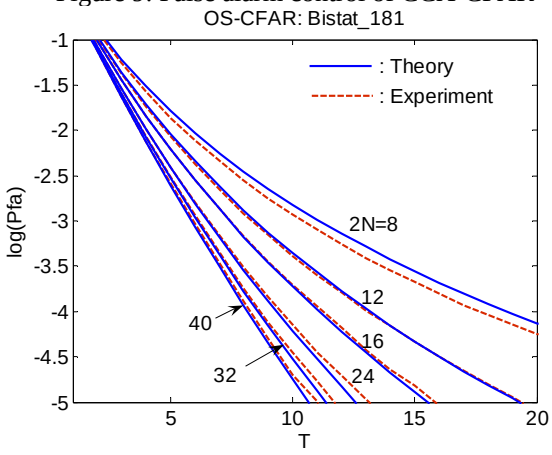

Figure 10: False alarm control of OS-CFAR

Acknowledgements

The authors would like to acknowledge the assistance of the Passive Bistatic Radar research team for their assistance in collecting and processing the datasets that were used in this article.

References

[1] M.I. Skolnik, Introduction to Radar Systems, McGraw-Hill Book Company, 2001, 3rd edn.

[2] P.P. Gandhi, S.A. Kassam, "Analysis of CFAR processors in nonhomogeneous background", IEEE Transactions on Aerospace & Electronic Systems, 1988, 24, (4), pp. 427-445.

[3] T.V. Cao and D. Sinnott, "A rare event approach to the detection of target-like signals in CFAR training data", Proc. the IET International Conference on Radar Systems, Edinburgh, UK, October 2007, pp1-5.

[4] T.V. Cao, "Design of low-loss CFAR detectors", Proc. the IEEE International Conference on Radar Systems, Adelaide, Australia, September 2008, pp712-717.

[5] T.V. Cao, "Constant false-alarm rate algorithm based on test cell information", IET Radar, Sonar, Navigation, 2008, vol. 2, No. 3, pp. 200-213.

[6] J. Palmer, D. Merrett, S. Palumbo, J. Piyaratna, S. Capon and H. Hansen, "Illuminator of opportunity bistatic radar research at DSTO", Proc. the IEEE International Conference on Radar Systems, Adelaide, Australia, September 2008, pp701-705.

[7] M. Sekine and Y. Mao, Weibull Radar Clutter, Peter Peregrinus Ltd., London, U.K. (on behalf of The Institution of Engineering and Technology), 1990.

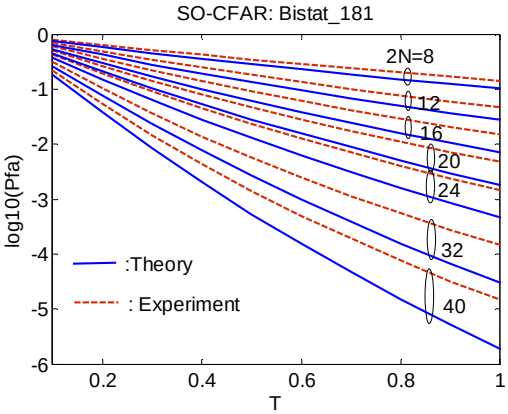

Figure 11: False alarm control of SO-CFAR

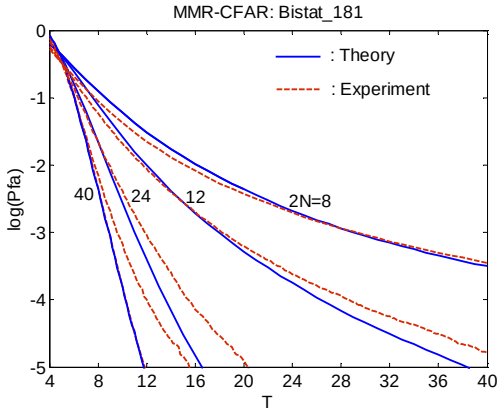

Figure 12: False alarm control of MMR test

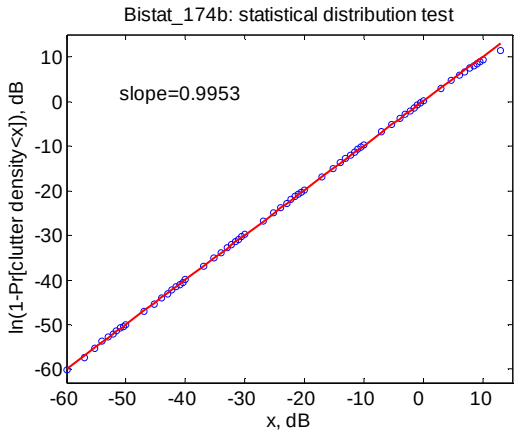

Figure 13: Statistical distribution of file Bistat_174b

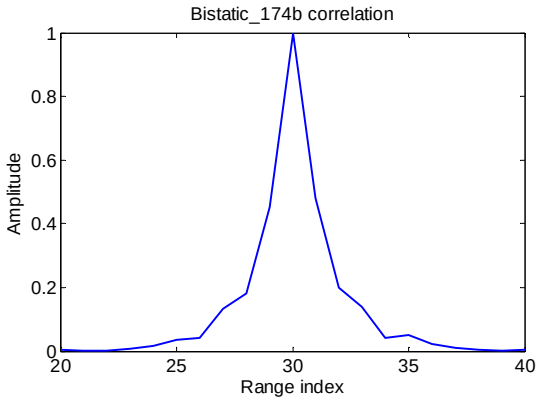

Figure 14: Range-delay correlation of file Bistat_174b

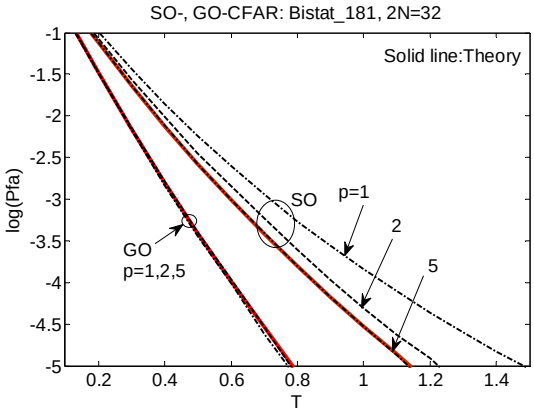

Figure 15: False alarm control of SO- and GO-CFAR